Electrochemistry | Hot Paper |

Cycling a Lithium Metal Anode at 90 °C in a Liquid Electrolyte

Li-Peng Hou, Xue-Qiang Zhang, Bo-Quan Li, and Qiang Zhang*

Abstract: *Stable operation at elevated temperature is necessary for lithium metal anode. However, Li metal anode generally has poor performance and safety concerns at high temperature (> 55°C) owing to the thermal instability of the electrolyte and solid electrolyte interphase in a routine liquid electrolyte. Herein a Li metal anode working at an elevated temperature (90°C) is demonstrated in a thermotolerant electrolyte. In a Li | LiFePO₄ battery working at 90°C, the anode undergoes 100 cycles compared with 10 cycles in a practical carbonate electrolyte. During the formation of the solid electrolyte interphase, independent and incomplete decomposition of Li salts and solvents aggravate. Some unstable intermediates emerge at 90°C, degenerating the uniformity of Li deposition. This work not only demonstrates a working Li metal anode at 90°C, but also provides fundamental understanding of solid electrolyte interphase and Li deposition at elevated temperature for rechargeable batteries.*

$\mathbf{W}$ith the increasing demands of portable electronics, electrical vehicles, and smart grids, secondary batteries with higher energy density compared with lithium (Li)-ion batteries are attracting much attention.[1] Li metal anode has been strongly considered as one of the most promising anode candidates for high-energy-density batteries with its merits of high theoretically specific capacity (3860 mAh g^{-1}) and low reduction potential (−3.04 V vs. standard hydrogen electrode).[2] In a practical perspective, the wide working temperature range is necessary for the secondary batteries owing to the diversified scenarios and working conditions,[3] especially an elevated temperature.[4]

Elevated temperature generally brings irreversible side reactions and even thermal runaway during the operation of a working battery.[5] A routine electrolyte in Li-ion batteries begins to decompose above 55 °C[6] and the solid electrolyte interphase (SEI) starts to disintegrate above 65 °C,[7] inducing a rapid degradation. The risk of thermal runaway increases rapidly beyond the working temperature range. This limits most Li-ion batteries only to work at a mild temperature range (< 55 °C).[5,8] While Li metal anode is employed, the high reactive nature of Li metal towards nonaqueous liquid electrolyte brings more severe and new challenges at elevated temperature. For example, the routine carbonate solvents with low boiling point (such as 126 °C for diethyl carbonate

(DEC)) will react with Li metal aggressively. Hydrogen fluoride (HF) induced by the hydrolysis of lithium hexafluorophosphate (LiPF₆) can increase significantly and corrode Li metal and SEI.[6] Therefore, a working Li metal anode at elevated temperature is much challenged but integrant for practical applications with diversified scenarios.

Pioneering efforts have been devoted to investigating the Li metal anode working at elevated temperature in a liquid electrolyte, such as electrolyte additives,[9] thermally stable solvents and Li salts,[10,11] and functional separators.[12] Recently, Li and co-workers demonstrated that Li metal batteries can deliver at 80 °C by employing two thermally stable Li salts, namely, lithium bis(trifluoro-methanesulfoni-mide) (LiTFSI) and lithium difluoro(oxalato)borate (LiDFOB), and ethylene carbonate (EC) and propylene carbonate (PC) solvents with high boiling point.[11] Apart from much improved cycling performance, the fundamental understanding in features of Li plating/stripping, the decomposition of electrolyte, and the formation of SEI at elevated temperature are worthy of attention.

When it comes to elevated temperature, the mechanical properties of Li metal and the reaction pathways between Li metal and electrolyte to form SEI will change. The yield strength of Li operated at 90 °C decreases by three orders of magnitude and the interfacial orientation of Li deposition alters, affording to new insights in suppressing Li dendrites.[13] Meanwhile, some chemical/electrochemical reactions, which cannot occur at room temperature (25 °C), will proceed at elevated temperature, enhancing the reaction and depletion of electrolyte and fresh Li metal. Furthermore, the kinetics of some decomposition reactions between Li and electrolyte can be accelerated with increasing temperature according to Arrhenius formula. Consequently, the components and structure of SEI change, inducing different Li ion diffusion pathways and the behaviors of Li deposition.[14,15] Therefore, a working Li metal anode at elevated temperature is much distinctive from that at room temperature. Furthermore, the exploration of a working Li metal anode at elevated temperature can provide new perspectives for disclosing the behaviors of Li plating/stripping and the formation mechanism of SEI, which affords fundamental guidance for anode interfacial regulation at elevated temperature in various battery systems.

Herein, a working Li metal anode is demonstrated at 90 °C in a thermotolerant liquid electrolyte. The better performance of Li metal anode at more elevated temperature induces less possibility of thermal runaway of batteries. Specially, lithium bis(fluorosulfonyl)imide (LiFSI) and lithium nitrate (LiNO₃) are dissolved in mixed solvents composed of fluoroethylene carbonate (FEC) and tetraethylene glycol dimethyl ether (TEGDME) to constitute an elevated temperature-tolerant (ET-tolerant) electrolyte. When applied

[*] L.-P. Hou, X.-Q. Zhang, B.-Q. Li, Prof. Q. Zhang
Beijing Key Laboratory of Green Chemical, Reaction Engineering and Technology, Department of Chemical Engineering
Tsinghua University, Beijing 100084 (P. R. China)
E-mail: zhang-qiang@mails.tsinghua.edu.cn

Supporting information and the ORCID identification number(s) for the author(s) of this article can be found under:
https://doi.org/10.1002/anie.202002711.

into a Li | LiFePO$_4$ battery working at 90°C, the Li metal anode undergoes 100 cycles in the ET-tolerant electrolyte with a capacity retention of 91.5%, while the Li metal anode rapidly degenerates only within 10 cycles in a practical routine electrolyte (1.0 M LiPF$_6$ in EC/DEC). Distinctive features of SEI and Li deposition at 90°C are revealed in the ET-tolerant electrolyte, which is a reasonable research platform. Both independent and incomplete decomposition of Li salts and solvents are enhanced at 90°C, altering the formation mechanisms of SEI at 25°C and inducing a degenerated uniformity of Li deposition.

The cycling performance of Li metal anode at 90°C is evaluated in Li | LiFePO$_4$ batteries. The full cells with the routine electrolyte fail rapidly within 10 cycles with a retention of 71.7% (Supporting Information, Figure S1a). The overcharge is obvious owing to the disintegration of electrolyte (Supporting Information, Figure S1b).[16] The low boiling point of DEC (126°C) and the decomposition of LiPF$_6$ above 55°C contribute to the fast capacity decay,[11] indicating that Li metal anode cannot tolerate cycling at 90°C in the practical carbonate electrolyte. Moreover, the carbonate electrolyte exhibits poor compatibility with Li metal, thus, the side effects can be enlarged at elevated temperature. Therefore, TEGDME,[17] an ether solvent with a high boiling point (275°C) and good compatibility with Li metal, and FEC,[18] which is generally considered to form a SEI to enhance the uniformity of Li deposition, are coupled as cosolvents in the ET-tolerant electrolyte. LiFSI, which is more thermally stable than LiPF$_6$, is employed as the Li salt.[19] Full cells with the ET-tolerant electrolyte deliver a prolonged lifespan with 91.5% capacity retention after 100 cycles, illustrating an absolute predominance over the routine carbonate electrolyte (Figure 1a). There is nearly no overcharge during repeated cycles (Figure 1b). Moreover, an overwhelming performance is achieved at room temperature in the ET-tolerant electrolyte (Supporting Information, Figure S2). Li | LiFePO$_4$ batteries with the ET-tolerant electrolyte exhibit a capacity retention of 93.8% after 500 cycles (1 C) at 25°C. The considerable performances both at 90 and 25°C illustrate that an enhanced Li metal anode can be achieved at a wide range of operation temperature. Nevertheless, the cycle stability of Li metal deteriorates when it comes to elevated temperature. Therefore, the evolution

behaviors of Li deposition and the formation mechanism of SEI at elevated temperature are required to be explored.

The interfacial evolution of a working Li metal anode at 90°C is detected by electrochemical impedance spectroscopy (EIS; Figure 2; Supporting Information, Figure S3). The semicircle in the high frequency and middle frequency region are designated to the resistance of Li ions through SEI (R_{SEI}) and charge transfer (R_{CT}), respectively.[20] Considering that LiFePO$_4$ is relatively stable during the electrochemical window of 2.5–4.0 V, the dominated interfacial impedance can be assigned to Li metal anode and SEI. The R_{SEI} increases about four times (from 35 to 150 ohm) after the first cycle at 90°C in the ET-tolerant electrolyte, indicating that high temperature promotes the generation of a high resistant SEI (Figure 2a,c). After the 10th cycle, the R_{SEI} exhibits a slight increase (from 150 to 195 ohm) accompanying with similar increase in R_{CT} (from 120 to 140 ohm). Although the SEI is highly resistant at 90°C, it maintains a mild stability during cycling. In contrast, much smaller and more stable R_{SEI} (35 and 31 ohm at the 1st and 10th cycle, respectively) is achieved in the ET-tolerant electrolyte when working at 25°C (Figure 2b,d). The increase of R_{SEI} in the same electrolyte but different temperatures implies that the increasing temperature alters the decomposition reactions between electrolyte and Li anode and changes the components and structure of SEI.
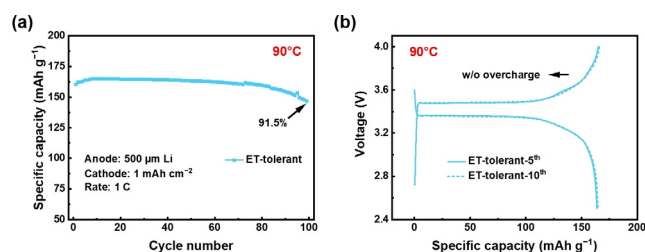

Figure 2. The evolution of interfacial resistance of Li | LiFePO$_4$ batteries using the ET-tolerant electrolyte during cycling at a),c) 90°C and b),d) 25°C. The dotted line is a local magnification of the impedance before cycling.

The homogeneity of Li plating/stripping and the accumulation of dead Li are efficient evidences for the uniformity of SEI.[21] Although local uniform Li deposition can be observed, the inhomogeneous utilization of active Li is still ubiquitous after the 10th cycle at 90°C (Figure 3a; Supporting Information, Figure S4a). Some areas of the pristine Li are not utilized during cycling. High temperature partially accelerates some side reactions between Li anode and electrolyte, and then results in enhanced inhomogeneity of SEI for Li ion diffusion. The nonuniform utilization patterns of Li metal is consistent with the previous works at 60°C in an ether electrolyte,[14,22]

Figure 1. Electrochemical performance of Li | LiFePO$_4$ batteries with an ET-tolerant electrolyte at 90°C. a) Cycle lifespan and b) corresponding voltage–capacity curves of Li | LiFePO$_4$ batteries. The Li | LiFePO$_4$ batteries with a Li metal anode of 500 μm and a cathode with an areal capacity of 1 mAh cm^{-2} were tested at 1 C (1 C = 170 mA g^{-1}).
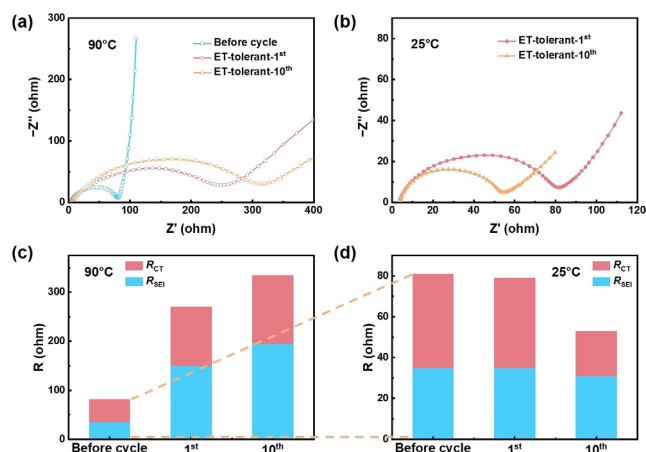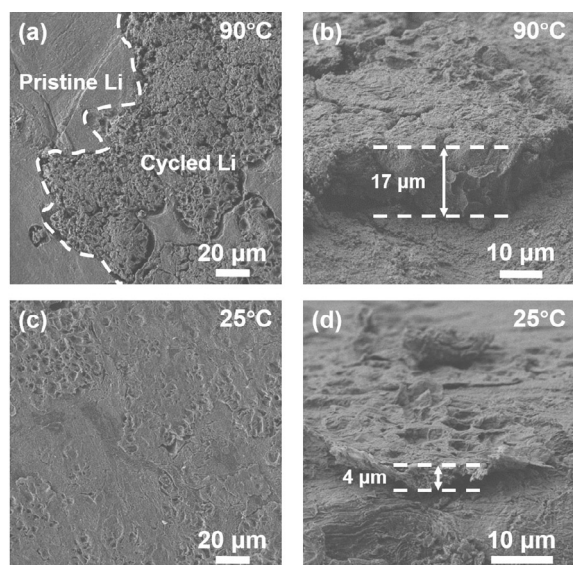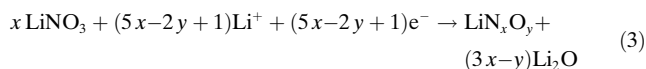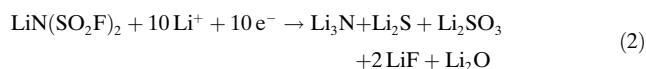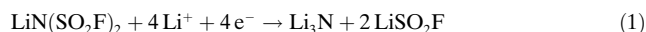
Figure 3. Top-sectional and cross-sectional morphologies of Li deposition in Li|LiFePO$_4$ batteries with the ET-tolerant electrolyte at a),b) 90°C and c),d) 25°C after the 10th cycle. Li metal anode was retrieved after cycled at 1 C. Pristine Li and Cycled Li in (a) represent the Li as received and the Li involved into cycling, respectively.

but the higher working temperature (90°C) induces new difference in Li deposition. The nonuniform Li utilization exacerbates the formation of dead Li layer, constructing an aggressive positive feedback and accelerating the repeated regeneration of SEI. Finally, a thick dead Li layer (ca. 17 μm) is formed only after 10 cycles when the operation temperature reaches 90°C (Figure 3b), which is related to a high resistance of SEI (Figure 2). When it comes to a moderate working temperature at 25°C, compact and uniform Li deposition with large Li nodules is observed (Figure 3c; Supporting Information, Figure S4b). The stable and low resistant SEI induces a thin dead Li layer ca. 4 μm after 10 cycles (Figure 3d). The behaviors of Li plating/stripping at 90°C is much more aggressive and beyond conventional cognition compared with that at 25°C.

The behaviors of Li plating/stripping are mainly related to the physical and chemical features of SEI. X-ray photoelectron spectroscopy (XPS) is conducted to reveal the evolution of the SEI formed at 90 or 25°C after etching for 1, 3, and 5 min on a Li anode surface (Figure 4). There is an abundant inorganic component of LiF throughout the whole SEI formed at 25°C, indicating a complete decomposition of FSI$^-$ (Figure 4a,g). LiF with high surface energy is generally regarded as an effective component for homogeneous and fast Li deposition,[23] which corresponds to the low R_{SEI} (Figure 2). In contrast, instead of LiF, the conspicuous existence of S–F bond can be detected at 90°C in F 1s spectra (Figure 4d). S–F species only originates from the disintegration of LiFSI. N–S bond in the FSI$^-$ is the weakest bond and S–F bond is the second weakest according to DFT calculations.[24] Therefore, the abundant S–F bond in SEI signifies that the decomposition of FSI$^-$ is incomplete at 90°C. Low content of LiF but much S–F species contributes to a relatively high resistant SEI at 90°C (Figure 2). The emergence of LiN$_x$O$_y$ both at

90°C and 25°C demonstrates that LiNO$_3$ involves in the formation of SEI (Figure 4b,e,h). Furthermore, the different species detected in S 2p spectra imply that high temperature alters the decomposition mechanism of FSI$^-$. As reported, NO$_3^-$ is considered to accelerate the decomposition of FSI$^-$ to sulfur-containing species in a high oxidation state, such as SO$_3^{2-}$ and SO$_4^{2-}$.[25] The ubiquitous distribution of SO$_3^{2-}$ and SO$_4^{2-}$ at different depths at 25°C demonstrates that the thorough decomposition of FSI$^-$ with the assistance of LiNO$_3$ (Figure 4c,i). Nevertheless, plentiful Li$_2$S and SO$_3^{2-}$ but little SO$_4^{2-}$ in S 2p spectra as well as abundant LiN$_x$O$_y$ in N 1s spectra detected at 90°C indicates that the disintegration of FSI$^-$ and NO$_3^-$ is separately enhanced at elevated temperature instead of NO$_3^-$ assisting the decomposition of FSI$^-$ to produce sulfur-containing species in a high oxidation state (Figure 4c,f). Moreover, the presence of organic C–F bond is detected at 90°C in F 1s spectra. The C–F bond only exists in FEC, which reveals that the incomplete decomposition of FEC participates in the formation of SEI with abundant organic components and less LiF. Therefore, the independent and incomplete disintegration of LiFSI and LiNO$_3$ are enhanced at 90°C and a possible decomposition mechanism of Li salts is proposed according to the results of XPS profiles by Equations (1), (2), and (3) (Supporting Information, Figure S5).

$$LiN(SO_2F)_2 + 4\,Li^+ + 4\,e^- \rightarrow Li_3N + 2\,LiSO_2F \tag{1}$$

$$LiN(SO_2F)_2 + 10\,Li^+ + 10\,e^- \rightarrow Li_3N + Li_2S + Li_2SO_3 \\ + 2\,LiF + Li_2O \tag{2}$$

$$x\,LiNO_3 + (5x-2y+1)Li^+ + (5x-2y+1)e^- \rightarrow LiN_xO_y + \\ (3x-y)Li_2O \tag{3}$$

According to the above analysis, a distinctive formation mechanism of SEI is proposed when Li metal anode is operated at elevated temperature in liquid electrolyte. On the one hand, the independent and incomplete decomposition of Li salts is enhanced at high working temperature. The intermediate products, such as LiN$_x$O$_y$ and components with S–F bond, generate at elevated temperature. Moreover, high temperature accelerates the decomposition process of NO$_3^-$, weakening the synergistic effect between NO$_3^-$ and FSI$^-$, which promotes specific spatial distribution of inorganic components in SEI. On the other hand, the incomplete disintegration of FEC solvent is enhanced at 90°C, forming more organic components (C–F species) instead of LiF. Less LiF with high surface energy induces a high interfacial impendence and non-uniformity of SEI at 90°C compared to that at 25°C. Consequently, a relatively nonuniform Li utilization can be observed at 90°C (Figure 5).

In conclusion, a working Li metal anode at 90°C is demonstrated in a thermotolerant electrolyte. A Li metal anode in Li|LiFePO$_4$ battery working at 90°C undergoes 100 cycles compared with 10 cycles in a routine electrolyte for practical batteries. The elevated temperature induces the independent and incomplete decomposition of Li salts and solvents, which significantly alters the components of SEI. Unstable intermediate decomposition products emerge but the components that contribute to rapid and uniform Li ion
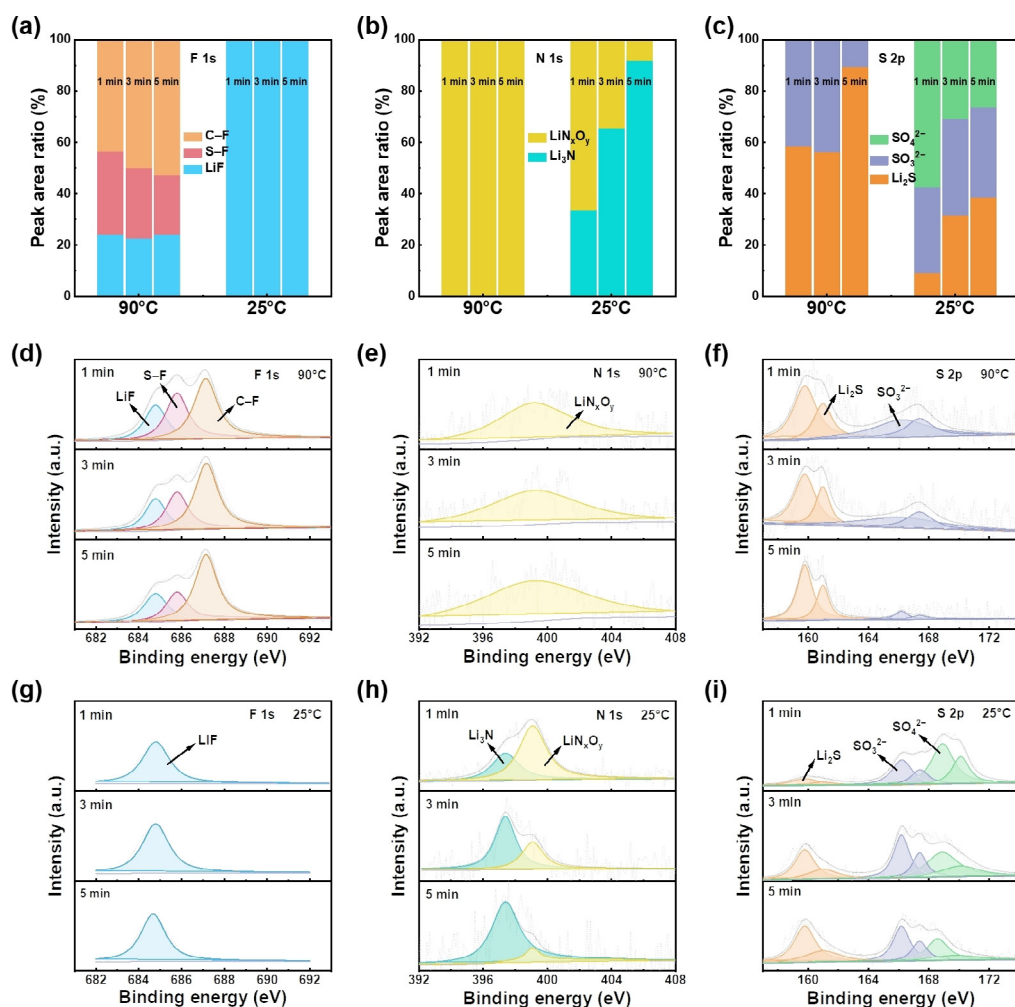
diffusion, such as LiF, decrease at 90 °C. Therefore, a high-resistance SEI forms and the resistance significantly varies spatially, which induces a non-uniform utilization of Li metal. This contribution not only demonstrates an unprecedented working Li metal anode at 90 °C but also affords a fresh fundamental understanding of SEI and Li deposition at elevated temperature for rechargeable batteries.

Figure 4. The analysis of the XPS spectra of SEI on Li anode at 90 and 25 °C after etching. a)–c) The peak area ratio retrieved from XPS spectra depth profiles of a) F 1s, b) N 1s, and c) S 2p spectra. d)–i) The corresponding XPS spectra depth profiles of Li anode at working temperature of d),e),f) 90 °C and g),h),i) 25 °C. The Li anode was received after the 10th cycle in Li | LiFePO₄ batteries tested at 1 C.

Conflict of interest

The authors declare no conflict of interest.

Keywords: elevated temperature · liquid electrolytes · lithium metal anodes · solid electrolyte interphase · thermal safety
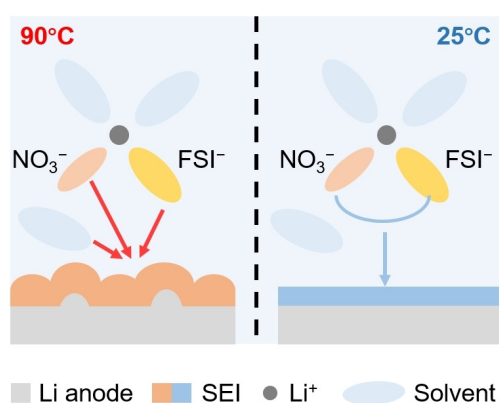

Figure 5. The SEI formation mechanisms at 90 and 25 °C. The independent and incomplete decomposition of FEC solvent, NO_3^-, and FSI^- are enhanced at 90 °C, inducing an inhomogeneous SEI and Li deposition (left). The thorough decomposition of FSI^- with the assistance of $LiNO_3$ is achieved at 25 °C, enabling a uniform SEI and Li deposition (right).

[1] H. Li, *Joule* **2019**, *3*, 911–914; X. Zeng, M. Li, D. Abd El-Hady, W. Alshitari, A. S. Al-Bogami, J. Lu, K. Amine, *Adv. Energy Mater.* **2019**, *9*, 1900161.

[2] P. G. Bruce, S. A. Freunberger, L. J. Hardwick, J.-M. Tarascon, *Nat. Mater.* **2012**, *11*, 19–29; X.-Q. Zhang, C.-Z. Zhao, J.-Q. Huang, Q. Zhang, *Engineering* **2018**, *4*, 831–847; Y. Liang, C. Z. Zhao, H. Yuan, Y. Chen, W. Zhang, J. Q. Huang, D. Yu, Y. Liu, M. M. Titirici, Y. L. Chueh, H. Yu, Q. Zhang, *InfoMat* **2019**, *1*, 6–32; X.-B. Cheng, C.-Z. Zhao, Y.-X. Yao, H. Liu, Q. Zhang, *Chem* **2019**, *5*, 74–96.

[3] X. Dong, Z. Guo, Z. Guo, Y. Wang, Y. Xia, *Joule* **2018**, *2*, 902–913; J. Kafle, J. Harris, J. Chang, J. Koshina, D. Boone, D. Qu, *J. Power Sources* **2018**, *392*, 60–68.

[4] X. Dong, Y. Lin, P. Li, Y. Ma, J. Huang, D. Bin, Y. Wang, Y. Qi, Y. Xia, *Angew. Chem. Int. Ed.* **2019**, *58*, 5623–5627; *Angew. Chem.* **2019**, *131*, 5679–5683; M.-T. F. Rodrigues, G. Babu, H. Gullapalli, K. Kalaga, F. N. Sayed, K. Kato, J. Joyner, P. M. Ajayan, *Nat. Energy* **2017**, *2*, 17108.

[5] H. Liu, Z. Wei, W. He, J. Zhao, *Energy Convers. Manage.* **2017**, *150*, 304–330.

[6] C. L. Campion, W. Li, B. L. Lucht, *J. Electrochem. Soc.* **2005**, *152*, A2327–A2334.

[7] Q. Wang, J. Sun, X. Yao, C. Chen, *J. Electrochem. Soc.* **2006**, *153*, A329–A333.

[8] K. Takada, Y. Yamada, A. Yamada, *ACS Appl. Mater. Interfaces* **2019**, *11*, 35770–35776.

[9] C. Xu, G. Hernandez, S. Abbrent, L. Kober, R. Konefal, J. Brus, K. Edstrom, D. Brandell, J. Mindemark, *ACS Appl. Energy Mater.* **2019**, *2*, 4925–4935.

[10] H. Yang, C. Guo, J. Chen, A. Naveed, J. Yang, Y. Nuli, J. Wang, *Angew. Chem. Int. Ed.* **2019**, *58*, 791–795; *Angew. Chem.* **2019**, *131*, 801–805; J. Wang, Y. Yamada, K. Sodeyama, E. Watanabe, K. Takada, Y. Tateyama, A. Yamada, *Nat. Energy* **2018**, *3*, 22–29.

[11] Z. Geng, J. Lu, Q. Li, J. Qiu, Y. Wang, J. Peng, J. Huang, W. Li, X. Yu, H. Li, *Energy Storage Mater.* **2019**, *23*, 646–652.

[12] Z. Zhou, T. Zhao, X. Lu, H. Cao, X. Zha, Z. Zhou, *J. Power Sources* **2018**, *396*, 542–550; Z. Zhou, B. Chen, T. Fang, Y. Li, Z. Zhou, Q. Wang, J. Zhang, Y. Zhao, *Adv. Energy Mater.* **2019**, *9*, 1902023.

[13] C. Xu, Z. Ahmad, A. Aryanfar, V. Viswanathan, J. R. Greer, *Proc. Natl. Acad. Sci. USA* **2017**, *114*, 57–61.

[14] Y. Han, Y. Jie, F. Huang, Y. Chen, Z. Lei, G. Zhang, X. Ren, L. Qin, R. Cao, S. Jiao, *Adv. Funct. Mater.* **2019**, *29*, 1904629.

[15] X. Sun, X. Zhang, Q. Ma, X. Guan, W. Wang, J. Luo, *Angew. Chem. Int. Ed.* **2020**, *59*, 6665–6674; *Angew. Chem.* **2020**, *132*, 6730–6739.

[16] K. Xu, *Chem. Rev.* **2014**, *114*, 11503–11618.

[17] K. Yoshida, M. Nakamura, Y. Kazue, N. Tachikawa, S. Tsuzuki, S. Seki, K. Dokko, M. Watanabe, *J. Am. Chem. Soc.* **2011**, *133*, 13121–13129; H. Yang, L. Yin, H. Shi, K. He, H.-M. Cheng, F. Li, *Chem. Commun.* **2019**, *55*, 13211–13214.

[18] H. Zhang, G. Gebresilassie Eshetu, X. Judez, C. Li, L. M. Rodriguez-Martinez, M. Armand, *Angew. Chem. Int. Ed.* **2018**, *57*, 15002–15027; *Angew. Chem.* **2018**, *130*, 15220–15246.

[19] F. Qiu, X. Li, H. Deng, D. Wang, X. Mu, P. He, H. Zhou, *Adv. Energy Mater.* **2018**, *8*, 1803372; T. T. Beyene, H. K. Bezabh, M. A. Weret, T. M. Hagos, C.-J. Huang, C.-H. Wang, W.-N. Su, H. Dai, B.-J. Hwang, *J. Electrochem. Soc.* **2019**, *166*, A1501–A1509.

[20] X. Q. Zhang, T. Li, B. Q. Li, R. Zhang, P. Shi, C. Yan, J. Q. Huang, Q. Zhang, *Angew. Chem. Int. Ed.* **2020**, *59*, 3252–3257; *Angew. Chem.* **2020**, *132*, 3278–3283; H. Xiang, P. Shi, P. Bhattacharya, X. Chen, D. Mei, M. E. Bowden, J. Zheng, J.-G. Zhang, W. Xu, *J. Power Sources* **2016**, *318*, 170–177.

[21] Y. Li, Y. Li, A. Pei, K. Yan, Y. Sun, C.-L. Wu, L.-M. Joubert, R. Chin, A. L. Koh, Y. Yu, J. Perrino, B. Butz, S. Chu, Y. Cui, *Science* **2017**, *358*, 506–510; Z. Peng, J. Song, L. Huai, H. Jia, B. Xiao, L. Zou, G. Zhu, A. Martinez, S. Roy, V. Murugesan, H. Lee, X. Ren, Q. Li, B. Liu, X. Li, D. Wang, W. Xu, J.-G. Zhang, *Adv. Energy Mater.* **2019**, *9*, 1901764.

[22] K. Yan, J. Wang, S. Zhao, D. Zhou, B. Sun, Y. Cui, G. Wang, *Angew. Chem. Int. Ed.* **2019**, *58*, 11364–11368; *Angew. Chem.* **2019**, *131*, 11486–11490.

[23] M. He, R. Guo, G. M. Hobold, H. Gao, B. M. Gallant, *Proc. Natl. Acad. Sci. USA* **2020**, *117*, 73–79; X.-Q. Zhang, X. Chen, X.-B. Cheng, B.-Q. Li, X. Shen, C. Yan, J.-Q. Huang, Q. Zhang, *Angew. Chem. Int. Ed.* **2018**, *57*, 5301–5305; *Angew. Chem.* **2018**, *130*, 5399–5403; T. Hou, G. Yang, N. N. Rajput, J. Self, S.-W. Park, J. Nanda, K. A. Persson, *Nano Energy* **2019**, *64*, 103881; S. Jurng, Z. L. Brown, J. Kim, B. L. Lucht, *Energy Environ. Sci.* **2018**, *11*, 2600–2608.

[24] R. Cao, J. Chen, K. S. Han, W. Xu, D. Mei, P. Bhattacharya, M. H. Engelhard, K. T. Mueller, J. Liu, J.-G. Zhang, *Adv. Funct. Mater.* **2016**, *26*, 3059–3066.

[25] X.-Q. Zhang, X. Chen, L.-P. Hou, B.-Q. Li, X.-B. Cheng, J.-Q. Huang, Q. Zhang, *ACS Energy Lett.* **2019**, *4*, 411–416; D. Aurbach, E. Pollak, R. Elazari, G. Salitra, C. S. Kelley, J. Affinito, *J. Electrochem. Soc.* **2009**, *156*, A694–A702; X. Chen, X. Q. Zhang, H. R. Li, Q. Zhang, *Batteries Supercaps* **2019**, *2*, 128–131.